Drag reduction properties of femtosecond laser-induced superhydrophobic dual-scale topographies

Anvesh Gaddam[1], Himani Sharma[2], Ratan Ahuja[3], Stefan Dimov[1], Suhas Joshi[3], Amit Agrawal[3]

[1]*Department of Mechanical Engineering, University of Birmingham, Edgbaston, Birmingham B15 2TT, UK*
[2]*Department of Chemical and Biomolecular Engineering, University of Notre Dame, Notre Dame, IN 46556, USA*
[3]*Department of Mechanical Engineering, Indian Institute of Technology Bombay, Mumbai, 400076, India*

Abstract

Despite the wide usage of non-Newtonian liquids in microfluidic devices, the drag reduction behaviour of such liquids was rarely examined in laminar flows in superhydrophobic (SH) textured microchannels. Here, we have investigated the influence of topologically different SH surfaces on drag reduction of shear-thinning liquids in microchannels. First, the flow enhancement factor on surface textures such as posts and ribs was estimated numerically over a range of flow rates as a function of microchannel constrictions and power-law index. Next, the dual-scale textured surfaces are fabricated by femtosecond laser processing on stainless steel and quantified the drag reduction properties of such SH surfaces in microchannels. The flow enhancement factor of shear-thinning liquids on the SH surfaces has exhibited non-monotonic variation with the applied flow rate. The maxima of the flow enhancement factor was noticed to differ with the constriction ratio, gas fraction and power-law index. Experiments were conducted with aqueous Xanthan Gum liquids in the SH microchannels. The flow enhancement factor has exhibited a non-monotonic behaviour and attenuated with an increase in power-law index similar to simulations. The results will provide useful insights into flow behaviour of shear-thinning liquids in SH microchannels.

Keywords: Carreau, femtosecond laser, LIPSS, shear-thinning, superhydrophobic, Xanthan Gum.

1. Introduction

Superhydrophobic (SH) micro and nanotextured surfaces have been a subject of significant interest in a plethora of applications such as self-cleaning [1], anti-biofouling [2] and anti-icing [3]. The velocity slip induced by the entrapped gas pockets on a rough SH surface reduces the pressure drop in the microchannels and thus alleviate the pumping power requirement in microfluidic devices [4]. However, most of the microfluidic devices operate with non-Newtonian liquids such as blood [5] and polymers [6]. Despite the importance of non-Newtonian liquids in microfluidics, the drag reduction of these liquids is rarely investigated in the context of flow through SH microchannels.

Haase et al. [7] investigated the behaviour of shear-thinning liquids on SH ribs in microchannels. The μ-PIV measurements revealed that the shear-thinning liquids exhibit significantly high drag reduction than the Newtonian liquids. Patlazhan et al. [8] studied a shear flow of shear-thinning liquids over ribs. Their numerical results confirmed that the drag reduction associated with the shear-thinning liquids is considerably larger than those with the Newtonian liquids. Crowdy et al. [9] corroborated these findings through the analytical investigation .

In addition, the SH textured surfaces for microfluidics are generally fabricated by time-intensive lithography-based techniques such as deep reactive ion etching and SU8-lithography. Moreover, these techniques are limited by material selectivity and footprint. For example, silicon is the preferred choice in wet-etching methods. Although the electrochemical micromachining methods are suitable for some metallic surfaces, they are limited by accuracy, feature size and involve harmful chemicals[10]. On the other hand, ultrashort pulse laser micromachining is a clean manufacturing technique to fabricate micro, nano and multiscale textures irrespective of any material [11].

In this work, we have numerically and experimentally investigated the flow behaviour of shear-thinning liquids in the pressure-driven flow through microchannels containing posts and ribs. The aqueous Xanthan Gum liquids are used as model shear-thinning liquids in both numerical simulations and experiments. In the experiments, the SH microchannels were prepared by femtosecond laser machining on stainless steel. Then, we have quantified and compared the flow enhancement of the shear-thinning liquids in microchannels with top and bottom walls covered with either posts or ribs, to those with smooth walls.

2. Methodology

2.1 Shear-thinning liquids

Three kinds of shear-thinning liquids were prepared by dissolving Xanthan Gum (Merck, Germany) in de-ionised water. The mass concentration of these aqueous Xanthan Gum (XG) solutions are 1, 2 and 5 g/L, which are designated as XG1, XG2 and XG5, respectively. The shear viscosity properties of these liquids were measured using a Anton-Paar rheometer. The viscosity variation for all the XG liquids is shown in Fig. 1, indicating the shear-thinning behaviour. The effective viscosity (η_{eff}) as a function of shear rate ($\dot{\gamma}$) of the XG liquids is expressed by Carreau model fit, given by Eq. 1.

$$\eta_{eff} = \eta_i + (\eta_o - \eta_i)[1 + (\lambda\dot{\gamma})^2]^{\frac{(n-1)}{2}} \quad (1)$$

Here, n is power law exponent, λ is relaxation time, η_i and η_o are the infinite and zero shear viscosities, respectively. The fitting parameters for each of the XG liquids are listed in table-1. These shear-thinning liquids were employed in the flow experiments in SH textured microchannels in this research.

Table-1 Carreau model parameters for the XG liquids of different mass concentrations.

Des.	g/L	η_i (Pa.s)	η_o (Pa.s)	n	λ (s)
XG1	1	0.089	0.0009	0.472	1.12
XG2	2	1.059	0.0011	0.312	3.41
XG5	5	5.078	0.0037	0.164	2.44

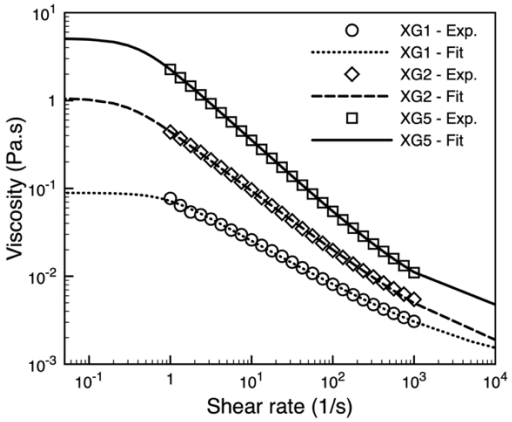

Fig. 1. Viscosity as a function of shear rate for aqueous XG solutions at different concentrations.

2.2 Numerical details

We examine two types of SH textures, namely, transverse ribs (TR) and posts as shown in Fig. 2. The liquid flows in an SH textured microchannel with a height of 2*H*. The unit cell has a size of *L* with the SH texture having a characteristic dimension of *s*. The constrictions ratio (*HL* = H/L) considered are 0.5 and 1, and the gas fraction (*GF*), which is a ratio of area covered by the liquid–gas interface to the total projected area, is varied at two levels, 0.5 and 0.9. The power-law index varied at three levels, 0.16, 0.32 and 0.48. Furthermore, the pressure-driven flow is considered to be fully developed and the liquid flows in the *x*-direction. Therefore, due to the periodically repeating flow field in the *x*-direction, the inlet and outlet of the computational domain are designated as the periodic boundaries. Since the microchannel is sufficiently wide (*z*-direction) exhibiting a 2D flow condition, the sidewalls of the domain are considered to be symmetric boundaries. Top wall of the domain is also considered as a symmetric boundary. Here, the liquid-gas interface (LGI) is assumed to be a shear-free boundary, while the solid-liquid interface (SLI) is considered as a no-slip boundary. All the simulations were performed in the Ansys Fluent 2020R1 framework. A velocity gradient-based adaption method in Fluent was used to obtain the grid independent solution. The refinement process continued until the continuity and velocity residuals reach 10^{-9}. The number of cells after refinement were ranged between 0.5-1 million. The pressure-velocity coupling was achieved through Coupled algorithm.

The applied pressure gradient, ($\Delta P/L$) was tuned corresponding to flow rate range of 0.3 to 100 mm^3/s for all microchannels irrespective of constriction ratio and power-law index. Finally, the flow enhancement factor was calculated using the following equation. Here, ε_s and ε_t are the flow rates in the smooth and SH textured microchannels, respectively.

$$\varepsilon = \frac{\varepsilon_t}{\varepsilon_s} - 1 \qquad (2)$$

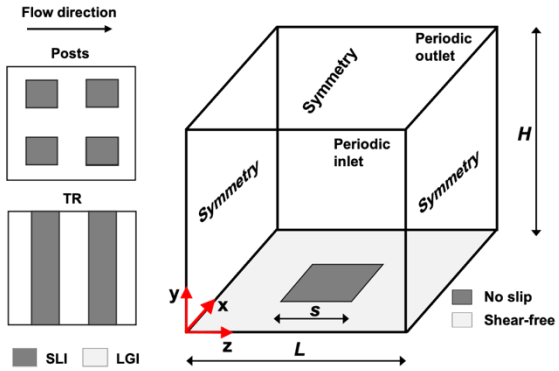

Fig. 2. Texture configurations and computational module with boundary conditions are shown.

2.3 Fabrication of microchannels and flow experiments

To assess the flow enhancement of XG liquids in SH textured microchannels, surfaces containing an array posts and ribs are fabricated by a femtosecond laser micromachining workstation (LASEA LS5, Belgium) on stainless steel (SS) 316L (1.4404). The femtosecond laser has a nominal wavelength of 1032 nm, average power of 5W, and a pulse energy of 10 µJ and a pulse duration of 310 fs. The beam was steered through a telecentric focusing lens and scanned at a speed of 1000 mm/s to create posts and ribs. The laser machining is performed at a repetition rate of 250 kHz. The scanning electron microscope (SEM, EOL JCM-600) images of the posts and ribs are shown in Fig. 3. They are further analysed through a focus variation microscope (Alicona G5) to obtain their dimensions. The 3D height map of the surface with posts together with its profile are shown in Fig. 3b. The distance/space between the posts is 75 µm and having a size of about 29 µm, which correspond to a gas fraction of ~ 85%. While, the spacing between the ribs is 100 µm with a size of about 15 µm, providing a gas fraction of ~ 85% on the surface. The side wall of the posts and ribs are in turn covered by the so-called laser-induced periodic surface structures (LIPSS). The LIPSS are nanoscale ripples with a periodicity of 800-900 nm and depth of 100-200 nm, as confirmed by our previous studies [2-3], which also help to resist the Cassie-Wenzel transition on SH textured surfaces as shown in Fig. 3.

The textured surfaces immediately after the laser processing exhibited a contact angle (CA) < 60°. They are further functionalised by applying Trichloro (1H,1H,2H,2H-perfluorooctyl) silane to impart the superhydrophobicity. The CA on the smooth and SH textured surfaces was measured using a goniometer (OCA 15EC, Data Physics GmbH, Germany). While the smooth surface exhibited a CA of 71.2° ± 2.9 with water, the contact angle on the SH textured surfaces was measured to be more than 150° both with water and XG liquids (see Fig. 3).

The smooth and SH textured microchannels were prepared on the same surface with the sticker technique. Briefly, an SS sheet was cut into two pieces of 25 mm x 100 mm size. In one half of each piece the SH textures were fabricated by femtosecond laser machining and silane functionalisation. Next, a slot of 2 mm x 70 mm was machined on a two-side adhesive plastic tape and bonded onto the SS sheets as shown in Fig. 4 to complete the microchannels.

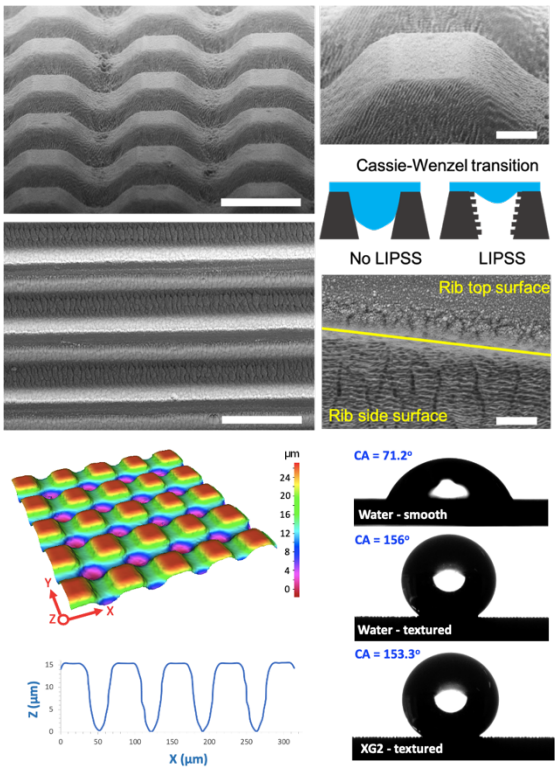

Fig. 3. (top) SEM micrograph of posts (scale bar: 50 μm) and ribs (scale bar: 100 μm). A magnified view of single posts and ribs showing LIPSS on side walls (scale bar: 10 μm). (bottom) Height map and profile of the posts are shown. Micrographs showing contact angle on smooth and SH textured surfaces.

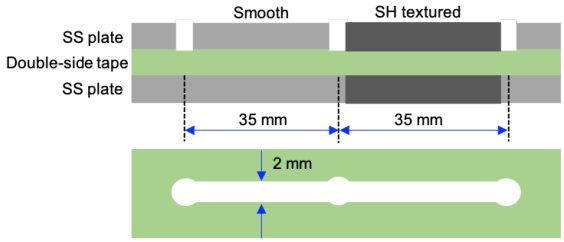

Fig. 4. An exploded view of the microchannel configuration employed for the experiments.

Therefore, the top and bottom walls of the SH textured microchannels were decorated with either posts or ribs. The microchannels with two heights were investigated using tapes with a thickness of 90 μm (Tesa 64621) and 200 μm (3M 9088). The XG liquids (XG1, XG2 and XG5) were fed through the microchannels with the same inlet using a syringe pump (Legato 110, KD Scientific) as shown in Fig. 4. The volume flow rate from smooth and SH textured microchannels was estimated by measuring the mass of the liquid collected from the outlets using a precision weighing balance. It should be noted that due to the shear-free boundary condition, the geometry of the textures below the top wall of ribs/posts is irrelevant. Thus, the experimental geometry can be equivalent to the numerical model.

3. Results and discussion

3.1 Flow enhancement estimation from simulations

Fig. 5 shows the flow enhancement factor as a function of an applied flow rate considering the effects of gas fraction, constriction ratio and power-law index. As can be seen, the enhancement factor is displaying a non-monotonic variation with the applied flow rate. The maxima of the enhancement factor is observed at an applied flow rate of 2.3 mm^3/s for a gas fraction of 0.9, irrespective of the constriction ratio for both ribs and posts. At the same time, enhancement factor is estimated to be more with posts than the ribs. On the other hand, a decrease in the gas fraction to 0.5 not only reduced the magnitude of the enhancement factor by two orders, but also shifted the maxima to the higher applied flow rates. Similarly, the weaker shear-thinning liquids (n=0.48), exhibited attenuated non-linearity of the enhancement factor when compared to the strongly shear-thinning liquids (n=0.16). Due to the continuous acceleration-deceleration cycles the liquid undergoes on slip and no-slip regions, the flow friction is higher in the case of ribs than the posts.

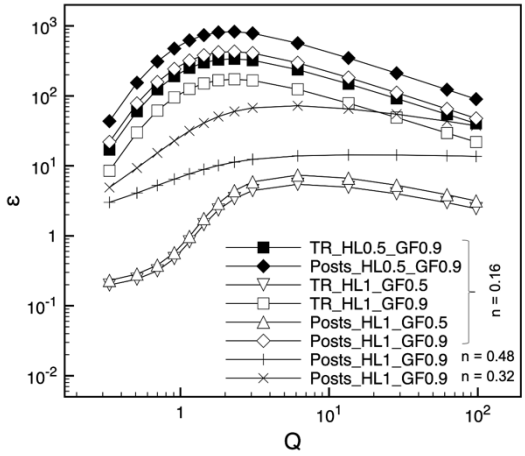

Fig. 5. Flow enhancement factor variation with flow rate at different constrictions ratios, gas fractions and power-law indices

3.2 Flow enhancement estimation from experiments

To validate the numerical results, water and shear-thinning liquids (XG1, XG2 and XG5) were fed through the smooth and SH textured microchannels with different heights and the flow enhancement factor was estimated using Eq. 2. Fig. 6 shows exemplary images of the quantity of liquid obtained in the smooth (right) and SH textured (left) microchannels with a height of 90 μm for the XG liquids. Here, the microchannels were fed with a flow rate of 8.33 mm^3/s. The flow rate obtained with the XG2 liquid in the smooth and SH textured microchannels 2.5 mm^3/s and 5.55 mm^3/s, respectively, and a flow rate of 1.94 mm^3/s and 6.11 mm^3/s, respectively for the XG5 liquid.

Fig. 7 quantifies the flow enhancement for the smooth and SH textured microchannels when fed with water and XG liquids for posts and ribs. As shown, the flow enhancement due to the SH textures is constant for the flow of water with respect to the smooth microchannels. While the posts resulted in a flow enhancement of 0.4 - 0.56, whereas the ribs showed an enhancement of 0.27 – 0.32 when the water is fed through the microchannels. On the other hand, the flow enhancement increases up to a flow rate of 0.83 mm^3/s and decreases thereafter for the XG2 and XG5 liquids in the microchannel with HL = 0.45 for both the posts and ribs. Since the XG5 liquid is strongly shear-thinning (n = 0.16) than the XG2 liquid (n = 0.31), the flow enhancement is found to be more in the former than the latter. For both liquids, the flow enhancement

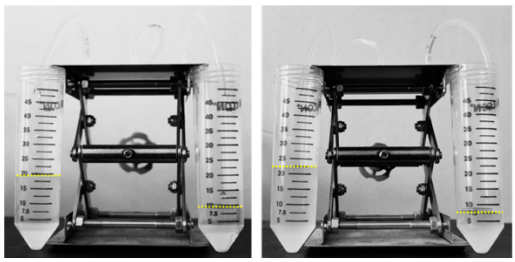

Fig. 6. Images showing flow rates in the SH microchannels with posts compared to the smooth microchannels for (left) XG2 (right) XG5 liquids.

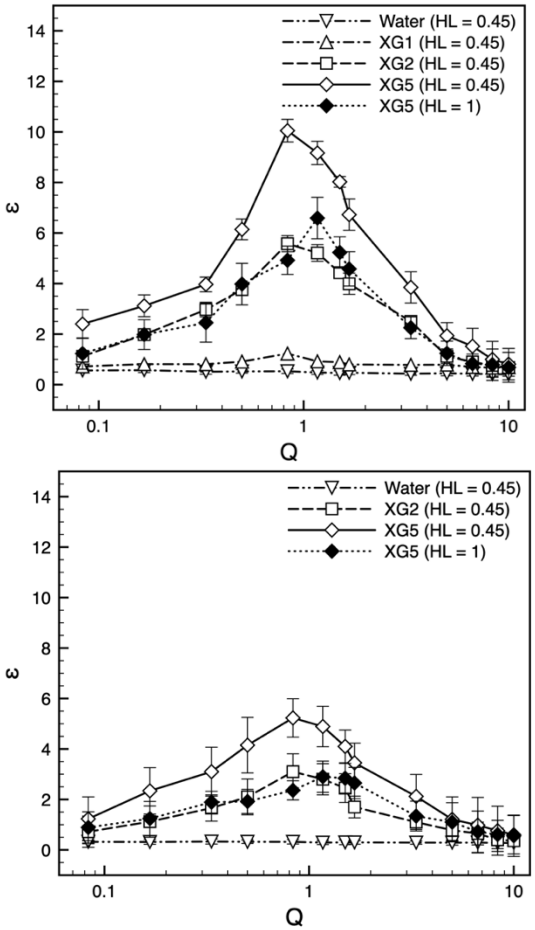

Fig. 7. Flow enhancement in microchannels with *HL* = 0.45, 1 and decorated with (top) posts and (bottom) transverse ribs as a function of the flow rate for water and XG liquids.

curves are plateauing towards the limit set by the water at low and high flow rates correspond to numerical simulations. At the same time, the ribs exhibited less enhancement than the posts, which is also in corroboration with the numerical results. However, the flow enhancement is noticed to be insignificant in the case of XG1 liquid for both posts and ribs, although it was marginally higher than the water in the former. This could be attributed to the weakly shear-thinning (n = 0.47) nature of the XG1 liquid as predicted by the numerical simulations. When the height of the microchannels is increased corresponding to *HL* = 1, the magnitude of the flow enhancement is decreased by 40% for the XG5 liquid, which also qualitatively corroborates the numerical estimates. It should be noted that numerical and experimental set-ups correspond to pressure-driven and mass-driven systems, thus the enhancement factors differ.

4. Conclusions

In this work, the flow behaviour of the shear-thinning liquids in flow through the SH textured microchannels in investigated in detail. The SH dual-scale topographies fabricated by the femtosecond laser are used to prepare the microchannels. Aqueous Xanthan Gum liquids when fed through the such SH microchannels containing posts and ribs led to a huge increase in the flow rate when compared to water. The experimental results were qualitatively in agreement with the numerical findings. In addition, the ultrafast lasers to fabricate drag reducing SH surfaces is also demonstrated in this work. The dual-scale structures are fabricated at a rate of 2 mm^2/s on metallic sheets but much higher processing speed can be achieved with high dynamics scanhead and laser sources. Therefore, ultrafast laser processing can be adopted to fabricate SH textures rapidly over large areas and on 3D/freeform surfaces where the drag reduction properties are needed, right from microfluidics to marine vehicles.

Acknowledgements

This research is conducted within the framework of the UKIERI-DST programme on ‘Surface functionalisation for food, packaging, and healthcare applications’ and the EU H2020 project HIMALAIA.

References

[1]. F.Geyer et al. “When and how self-cleaning of superhydrophobic surfaces works”. Sci. Adv., 2020, 6(3), p.eaaw9727.

[2]. R.Y.Siddiquie et al. “Anti-biofouling properties of femtosecond laser-induced submicron topographies on elastomeric surfaces”. Langmuir, 36(19), pp.5349-5358.

[3]. A.Gaddam et al. “Anti-icing properties of femtosecond laser-induced nano and multiscale topographies”. Appl. Surf. Sci., 2021, p.149443.

[4]. A.M.Davis et al. “ Geometric transition in friction for flow over a bubble mattress”. Phys. Fluids, 2009, 21(1), p.011701.

[5]. V. Laxmi et al. “Separation and Enrichment of Platelets from Whole Blood Using a PDMS-Based Passive Microdevice”. Ind. Eng. Chem. Res., 2020, *59*(10), pp.4792-4801.

[6]. M.A.Raoufi et al. “Experimental and numerical study of elasto-inertial focusing in straight channels”. Biomicrofluidics, 2019,*13*(3), p.034103.

[7]. A.S.Haase et al. “Inelastic non-Newtonian flow over heterogeneously slippery surfaces”. Phys. Rev. E, 2017, *95*(2), p.023105.

[8]. S. Patlazhan et al. “Apparent slip of shear thinning fluid in a microchannel with a superhydrophobic wall”. Phys. Rev. E, 2017, 96(1), p.013104.

[9]. D. Crowdy. “Effect of shear thinning on superhydrophobic slip: Perturbative corrections to the effective slip length”. Phys. Rev. Fluids, 2017, *2*(12), p.124201.

[110]. D. Dilip, “Sustained drag reduction and thermo-hydraulic performance enhancement in textured hydrophobic microchannels”. Int. J. Heat and Mass Transf., 2018 *119*, pp.551-563.

[11]. E. Stratakis et al. “Laser engineering of biomimetic surfaces”. Mater. Sci. Eng. R Rep., 2020, *141*, p.100562.